Indian J. pure appl. Math., **13**(10) : 1172-1191, October 1982

MATHEMATICAL SIMULATION OF UNSTEADY BLOOD FLOW IN BRANCHED ARTERIES

P. K. SURI

Computer Centre, Kurukshetra University, Kurukshetra 132119

AND

P. D. S. VERMA

Department of Mathematics, Regional Engineering College, Kurukshetra 132119

(*Received* 3 *October* 1981)

The aim of this work is to present blood flow patterns and the development of high shear forces at arterial walls near the apex of bifurcation. The study was motivated by medical research on the occurrence of cardiovascular lesions in branching flows for the living system under different circumstances. Here, the unsteady flow of blood in two-dimensional bifurcation with a symmetrical flow divider at different Reynolds number is discussed. The mathematical expressions for (i) velocity components, pressure gradient parameter, (ii) shear stresses at the inner and outer walls of bifurcation, and (iii) blockage effect at the apex of bifurcation have been computed to discuss and analyse this model. By using the initial conditions, the derivations obtained for unsteady flow in a branch reduces to the steady case as obtained by Zamir and Roach (1973).

1. INTRODUCTION

Blood flow problems in branched arteries has an increasing interest due to occurrence of certain vascular lesions which tend to occur near the junction of arterial network in the human system. Such lesions are atherosclerosis (a generic term covering a number of diseases of blood vessels like atherosclerotic plaques, intimal cushions and aneurysms etc.) These are of great clinical importance because of their predilection for coronary, cerebral and peripheral arteries. Such lesions develop insidiously and are probably caused by both environmental and hereditary factors. In atherosclerosis, there is hyalinization of small arteries, usually secondary to hypertension; and involutional changes, which accompany the increasing age and are characterized by loss of elastic tissue, spotty calcification and intimal thickening. Atherosclerotic plaques are characterized by intimal thickening due to localized accumulation of lipids and subintimal fatty changes. Aneurysms result from focal weakness and distension of blood vessel which occur most common in ascending portion of the thoracic aorta and at the apex of bifurcation in the 'circle of Willis' of brain circulation system. The intimal cushions are characterized by a proliferation of muscle and fibrous tissue at the outer walls of bifurcation.

Many authors have concluded, in their respective studies theoretically and experimentally, that the hemodynamic forces may be important in the pathogenesis

of cardiovascular and neural lesions. Earlier Forbus (1930), Hassler (1963), Pool and Potts (1965) and many other workers believed that intracranial saccular aneurysms are the result of congential defects in the media at the bifurcation of intracranial arteries; but later Ferguson (1972) observed that aneurysms are probably produced by hemodynamic forces. Stehbens (1959, 1961) and Schroter and Sudlow (1969) in their respective bifurcating models have shown that complex flow patterns arise at the apex of bifurcation and while eddies and turbulence was observed in the proximal portion of branch points. Further, Roach *et al.* (1972) reviewed in their glass model studies that the hemodynamic forces are responsible in the generation of various type of lesions in 'circle of Willis' of the brain circulation system particularly.

This work deals with unsteady flow of blood in a two-dimensional bifurcating model (geometry as chosen by Zamir and Roach 1973) to analyse and discuss hemodynamic factors mathematically, which are responsible in the development of arterial lesions such as aneurysms, arteriosclerosis and intimal cushions, etc.

2. Model Description

In the real human system, arterial and venual networks have complex three-dimensional distensible tubes which are not of uniform area af cross-section, nor are corners sharp. The angle of bifurcation in the branched arteries vary too much. Arterial junction geometries are not fixed because the elastic walls yield to the unsteady pressure pulses of the flowing blood. Also blood is not in fact a Newtonian fluid, but a viscoelastic suspension of R.B.C., W.B.C. and other blood cells. For mathematical convenience, a two-dimensional bifurcation model of similar geometry shown in Fig. 1, as taken by Zamir and Roach (1973) in their model, was selected

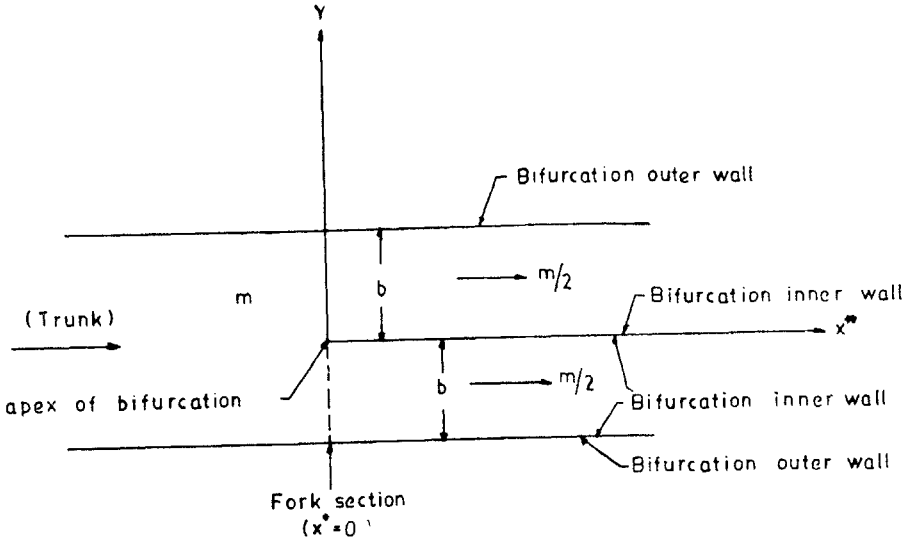

FIG. 1. Unsteady flow of blood through a bifurcation.

to provide analysis for unsteady blood flow in branch dynamics superseding their analysis for steady flow. In the present attempt, blood is considered to be Newtonian, incompressible, homogeneous and viscous fluid flowing in a non-conducting parallel plate channel in such a way that the flow is from trunk to the branches. The rate of mass flow at any cross-section perpendicular to the direction of flow is $m=2b\rho V$, where V is the mean velocity of flow, b is branch diameter and ρ is blood density. To simplify, the angle of bifurcation is taken to be zero so that a parallel stream is divided into two streams. In addition, thickness of the bifurcating wall is considered to be negligibly small in order to have the rate of mass flow at any cross-section of branched channel as $m/2$. Since the breadth of the channel under consideration (which is parallel to large artery) is much larger than 1mm, the viscosity of blood can be treated as constant throughout this analysis—that is by ignoring the Fahreus-Lindquist effect.

3. Governing Equations of Flow

In the present problem shown in Fig. 1, the unsteady flow is in the direction of x^*, i.e. from trunk to the branches, and the rate of mass flow at any cross-section perpendicular to x^* is m. If we take u^* and v^* as velocity components at any point in the flow field at time t^*, then by introducing the term $\partial u^*/\partial t^*$ for unsteady flow, the flow is governed by the two-dimensional boundary layer equations:

$$\frac{\partial u^*}{\partial t^*}+u^*\frac{\partial u^*}{\partial x^*}+v^*\frac{\partial u^*}{\partial y^*}+\frac{1}{\rho}\frac{dp^*}{dx^*}=\frac{\eta}{\rho}\left(\frac{\partial^2 u^*}{\partial y^{*2}}\right) \qquad \ldots(1)$$

$$\frac{\partial u^*}{\partial x^*}+\frac{\partial v^*}{\partial y^*}=0. \qquad \ldots(2)$$

For convenience, we define the following non-dimensional quantities:

$$x=\frac{x^*}{b},\ u=\frac{u^*}{(m/2b\rho)},\ h(x,t)=\frac{(dp^*/dx^*)}{(\eta m/2b^3\rho)},\ R=\frac{m}{2\eta},$$

$$y=\frac{y^*}{b},\ v=\frac{v^*}{(m/2b\rho)},\ \text{and}\ t=\frac{t^*}{(b^2\rho/\eta)}, \qquad \ldots(3)$$

Substituting these above defined parameters [eqn. (3)] into the flow equations (1) and (2), we get the dimensionless equations as

$$\frac{1}{R}\frac{\partial u}{\partial t}+u\frac{\partial u}{\partial x}+v\frac{\partial u}{\partial y}+\frac{1}{R}h(x,t)=\frac{1}{R}\frac{\partial^2 u}{\partial y^2} \qquad \ldots(4)$$

$$\frac{\partial u}{\partial x}+\frac{\partial v}{\partial y}=0. \qquad \ldots(5)$$

Here, we use a perturbation method for solving eqns. (4) and (5) governing blood flow through a bifurcation that a time dependent flow of physical importance is generated by main stream flows (as considered by Lighthill 1954) so that

$$\left.\begin{aligned} u(x,y,t) &= u_0(x,y)+\epsilon\, u_1(x,y)\, e^{int} \\ v(x,y,t) &= v_0(x,y)+\epsilon\, v_1(x,y)\, e^{int} \\ h(x,t) &= h_0(x)+\epsilon\, h_1(x,y)\, e^{int} \end{aligned}\right\} \qquad \ldots(6)$$

where the perturbation parameter ϵ is very small and hence we can assume square and higher order terms of ϵ to be of negligibly small magnitude) and n is the pulse rate.

Substituting (6) in (4) and (5), and comparing the coefficients of zero and first order terms of ϵ on both sides, we obtain

$$u_0 \frac{\partial u_0}{\partial x} + v_0 \frac{\partial u_0}{\partial y} = \frac{1}{R}\left[\frac{\partial^2 u_0}{\partial y^2} - h_0\right] \qquad ...(7)$$

$$u_0 \frac{\partial u_1}{\partial x} + u_1 \frac{\partial u_0}{\partial x} + v_1 \frac{\partial u_0}{\partial y} + v_0 \frac{\partial u_1}{\partial y} = \frac{1}{R}\left[\frac{\partial^2 u_1}{\partial y^2} - h - inu_1\right] \qquad ...(8)$$

$$\frac{\partial u_0}{\partial x} + \frac{\partial v_0}{\partial y} = 0 \qquad ...(9)$$

and

$$\frac{\partial u_1}{\partial x} + \frac{\partial v_1}{\partial y} = 0. \qquad ...(10)$$

Initial and Boundary Conditions

(a) Initially at $t = 0$, we have

$$u = u_0 + \epsilon u_1, \; v = v_0 + \epsilon v_1, \; h = h_0 + \epsilon h_1, \qquad ...(11)$$

where ϵ is the perturbation parameter.

(b) The boundary conditions in the trunk and branches are such 'no-slip' conditions that

for $x < 0$ (trunk); $u(x,y,t) = v(x,y,t) = 0$ on $y = \pm 1$, ...(12)

and for $x \geqslant 0$ (branches); $u(x,y,t) = v(x,y,t) = 0$ on $y = 0, \pm 1$. ...(13)

Further, we postulate that the flow far away from either side of the apex of bifurcation becomes fully developed Poiseuille flow such that as $x \to -\infty$;

$$u \to \frac{3}{2}(1-y^2)(1 + \epsilon \cos nt), \; v \to 0, \qquad ...(14)$$

$$h \to n \in \sin nt - 3(1 + \epsilon \cos nt),$$

and as $x \to +\infty$;

$$u \to 6(y - y^2)(1 + \epsilon \cos nt), \text{ for } y > 0$$

$$u \to -6(y + y^2)(1 + \epsilon \cos nt), \text{ for } y < 0 \qquad ...(15)$$

$$v \to 0, \; h \to n \in \sin nt - 12(1 + \epsilon \cos nt).$$

In addition to it, the law of conservation of mass is preserved by the dimensionless equation

$$\int_0^1 u(x,y,t)\, dy = 1. \qquad ...(16)$$

4. Solution

Momentum and moment of momentum integral method is more important in the present analysis, as the pressure gradient parameter is unknown, so it is appropriate

priate to analyse the solution based on integral form of the boundary layer equations. Further, since the flow is symmetrical, it is sufficient to restrict our analysis to one of the branches i.e., the region bounded by

$$0 \leqslant x \leqslant +\infty, 0 \leqslant y \leqslant +1. \qquad \ldots(17)$$

From eqns. (9) and (10), we have

$$v_0 = -\int_0^y \frac{\partial u_0}{\partial x}\, dy \qquad \ldots(18)$$

$$v_1 = -\int_0^y \frac{\partial u_1}{\partial x}\, dy \qquad \ldots(19)$$

where y is any point between 0 and 1.

Using (18) and (19), eqns. (7) to (10) can be combined to give the following equations:

$$u_0 \frac{\partial u_0}{\partial x} - \frac{\partial u_0}{\partial y}\int_0^y \frac{\partial u_0}{\partial x}\, dy + \frac{h_0}{R} = \frac{1}{R}\frac{\partial^2 u_0}{\partial y^2} \qquad \ldots(20)$$

$$u_0 \frac{\partial u_1}{\partial x} + u_1 \frac{\partial u_0}{\partial x} - \frac{\partial u_0}{\partial y}\int_0^y \frac{\partial u_1}{\partial x}\, dy - \frac{\partial u_1}{\partial y}\int_0^y \frac{\partial u_0}{\partial x}\, dy + \frac{h_1}{R} + \frac{in\, u_1}{R} = \frac{1}{R}\frac{\partial^2 u_1}{\partial y^2} \qquad \ldots(21)$$

which govern momentum in the x-direction.

The additional two equations, which govern the moment of momentum in the x-direction, can be obtained by multiplying the eqns. (20) and (21) throughout by y to get, respectively,

$$y\, u_0 \frac{\partial u_0}{\partial x} - y\, \frac{\partial u_0}{\partial y}\int_0^y \frac{\partial u_0}{\partial x} dy + y\, \frac{h_0}{R} = \frac{y}{R}\frac{\partial^2 u_0}{\partial y^2} \qquad \ldots(22)$$

$$y\, u_0 \frac{\partial u_1}{\partial x} + y u_1 \frac{\partial u_0}{\partial x} - y \frac{\partial u_0}{\partial y}\int_0^y \frac{\partial u_1}{\partial x} dy - y \frac{\partial u_1}{\partial y}\int_0^y \frac{\partial u_0}{\partial x} dy + y\, \frac{h_1}{R} + \frac{in\, y\, u_1}{R} = \frac{y}{R}\frac{\partial^2 u_1}{\partial y^2}. \qquad \ldots(23)$$

Integral forms of the boundary layer equations can be obtained by integrating each term in eqns. (20) to (23) from $y = 0$ to $y = 1$ (for one of the branched channel), to get, respectively,

$$\int_0^1 u_0 \frac{\partial u_0}{\partial x}\, dy - \int_0^1 \left(\frac{\partial u_0}{\partial y}\int_0^y \frac{\partial u_0}{\partial x} dy\right) dy + \frac{h_0}{R}\int_0^1 dy = \frac{1}{R}\int_0^1 \frac{\partial^2 u_0}{\partial y^2}\, dy \qquad \ldots(24)$$

$$\int_0^1 u_0 \frac{\partial u_1}{\partial x}\,dy + \int_0^1 u_1 \frac{\partial u_0}{\partial x}\,dy - \int_0^1 \left(\frac{\partial u_0}{\partial y} \int_0^y \frac{\partial u_1}{\partial x}\,dy \right) dy - \int_0^1 \left(\frac{\partial u_1}{\partial y} \int_0^y \frac{\partial u_0}{\partial x}\,dy \right) dy$$

$$+ \frac{h_1}{R} \int_0^1 dy + \frac{in}{R} \int_0^1 u_1\,dy = \frac{1}{R} \int_0^1 \frac{\partial^2 u_1}{\partial y^2}\,dy \qquad \ldots(25)$$

$$\int_0^1 y\,u_0 \frac{\partial u_0}{\partial x}\,dy - \int_0^1 \left(y \frac{\partial u_0}{\partial y} \int_0^y \frac{\partial u_0}{\partial x}\,dy \right) dy + \frac{h_0}{R} \int_0^1 y\,dy = \frac{1}{R} \int_0^1 y \frac{\partial^2 u_0}{\partial y^2}\,dy \qquad \ldots(26)$$

and

$$\int_0^1 y\,u_0 \frac{\partial u_1}{\partial x}\,dy + \int_0^1 y\,u_1 \frac{\partial u_0}{\partial x}\,dy - \int_0^1 \left(y \frac{\partial u_0}{\partial y} \int_0^y \frac{\partial u_1}{\partial x}\,dy \right) dy - \int_0^1 \left(y \frac{\partial u_1}{\partial y} \int_0^y \frac{\partial u_0}{\partial x}\,dy \right) dy$$

$$+ \frac{h_1}{R} \int_0^1 y\,dy + \frac{in}{R} \int_0^1 y\,u_1\,dy = \frac{1}{R} \int_0^1 y \frac{\partial^2 u_1}{\partial y^2}\,dy. \qquad \ldots(27)$$

Now integrating term by term (by parts), these equations from (24) to (27) can further be simplified as under to get, respectively,

$$2 \int_0^1 u_0 \frac{\partial u_0}{\partial x}\,dy + \frac{h_0}{R} = \frac{1}{R} \left[\left(\frac{\partial u_0}{\partial y} \right)_{y=1} - \left(\frac{\partial u_0}{\partial y} \right)_{y=0} \right] \qquad \ldots(28)$$

$$2 \int_0^1 u_0 \frac{\partial u_1}{\partial x}\,dy + 2 \int_0^1 u_1 \frac{\partial u_0}{\partial x}\,dy + \frac{h_1}{R} + \frac{in}{R} \int_0^1 u_1\,dy$$

$$= \frac{1}{R} \left[\left(\frac{\partial u_1}{\partial y} \right)_{y=1} - \left(\frac{\partial u_1}{\partial y} \right)_{y=0} \right] \qquad \ldots(29)$$

$$2 \int_0^1 y\,u_0 \frac{\partial u_0}{\partial x}\,dy + \int_0^1 \left(u_0 \int_0^y \frac{\partial u_0}{\partial x}\,dy \right) dy + \frac{h_0}{2R} = \frac{1}{R} \left(\frac{\partial u_0}{\partial y} \right)_{y=1} \qquad \ldots(30)$$

$$2 \int_0^1 y\,u_0 \frac{\partial u_1}{\partial x}\,dy + 2 \int_0^1 y\,u_1 \frac{\partial u_0}{\partial x}\,dy + \int_0^1 \left(u_0 \int_0^y \frac{\partial u_1}{\partial x}\,dy \right) dy + \int_0^1 \left(u_1 \int_0^y \frac{\partial u_0}{\partial x}\,dy \right) dy$$

$$+ \frac{h_1}{2R} + \frac{in}{R} \int_0^1 y\,u_1\,dy = \frac{1}{R} \left(\frac{\partial u_1}{\partial y} \right)_{y=1} \qquad \ldots(31)$$

which are the final momentum and moment of momentum Integral equations to be solved.

Since the integral equations (28) to (31) contain four unknowns h_0, h_1, u_0 and u_1 of which h_0, h_1 are functions of x only and while u_0 and u_1 are functions of both x and y, so it is appropriate to choose the solutions for u_0 and u_1 of the third degree polynomial form as

$$u_0 = f_0 + y f_1(x) + y^2 f_2(x) + y^3 g(x) \quad ...(32)$$

$$u_1 = F_0 + y F_1(x) + y^2 F_2(x) + y^3 G(x) \quad ...(33)$$

where f_0, f_1, f_2, g, F_0, F_1, F_2 and G are arbitrary functions of x. These unknowns can be obtained by substituting the conditions (13) and (16) into the eqns. (32) and (33), to get

$$f_0 = 0,\ f_1 = \left(6 + \frac{1}{2} g\right), f_2 = -\left(6 + \frac{3}{2} g\right);$$

$$F_0 = 0,\ F_1 = \left(6 + \frac{1}{2} G\right) \text{ and } F_2 = -\left(6 + \frac{3}{2} G\right). \quad ...(34)$$

Thus the assumed polynomial solutions in terms of unknowns $g(x)$ and $G(x)$ become

$$u_0 = 6\,(y - y^2) + \left(y^3 - \frac{3}{2} y^2 + \frac{1}{2} y\right) g \quad ...(35)$$

and

$$u_1 = 6\,(y - y^2) + \left(y^3 - \frac{3}{2} y^2 + \frac{1}{2} y\right) G. \quad ...(36)$$

Substituting (35) and (36) into the momentum integral equations (28) to (31), we get

$$g\,g' + \frac{420}{R}\,(h_0 + 12) = 0 \quad ...(37)$$

$$g\,g' - 3g' + \frac{420}{R}\,(h_0 + 12 - g) = 0 \quad ...(38)$$

$$g\,G' - g'\,G + \frac{420}{R}\,(h_1 + in + 12) = 0 \quad ...(39)$$

$$(g\,G' + g'\,G) - 3\,(g' + G') + \frac{420}{R}\left[h_1 + 12 + in - G\left(1 + \frac{in}{60}\right)\right] = 0 \quad ...(40)$$

where g' and G' are differentiation of the functions g and G with respect to x. Now eliminating h_0 from eqns. (37) and (38), and h_1 from eqns. (39) and (40), we find first order differential equations as

$$g' + \left(\frac{140}{R}\right) g = 0 \quad ...(41)$$

and

$$(g' + G') + \frac{140\,G}{R}\left(1 + \frac{in}{60}\right) = 0 \quad ...(42)$$

which has solutions

$$g = g_0 \, e^{-(140/R)x} \qquad \ldots(43)$$

and

$$G = e^{-7(in+60)x/3R}\left[G_0 + \frac{i\,60\,g_0}{n}\left(1 - e^{7inx/3R}\right)\right], \qquad \ldots(44)$$

respectively.

Putting the values of g and G in eqns. (35) and (36) respectively, the expression for u_0 and u_1 becomes

$$u_0 = 6\,(y - y^2) + \left(y^3 - \frac{3}{2}y^2 + \frac{y}{2}\right) g_0 \, e^{-(140/R)x} \qquad \ldots(45)$$

$$u_1 = 6\,(y - y^2) + \left(y^3 - \frac{3}{2}y^2 + \frac{y}{2}\right) e^{-7(in+60)x/3R} \times \left[G_0 + \frac{i\,g_0\,60}{n}\left(1 - e^{-7inx/3R}\right)\right] \qquad \ldots(46)$$

and thus consequently from eqns. (18) and (19), v_0 and v_1 can be obtained respectively as :

$$v_0 = \frac{35}{R}(y^4 - 2y^3 + y^2)\, g_0 \, e^{-(140/R)x} \qquad \ldots(47)$$

$$v_1 = (y^4 - 2y^3 + y^2)\, e^{-7(in+60)x/3R}\left[\frac{7\,(in + 60)}{12R} \times \left[G_0 + \frac{60ig_0}{n}\left(1 - e^{7inx/3R}\right)\right] - \frac{35}{R}\, g_0 \, e^{7inx/3R}\right]. \qquad \ldots(48)$$

From (43) and (44), we have

$$g' = -\,(140/R)\, g_0 \, e^{-(140/R)x} \qquad \ldots(49)$$

and

$$G' = -\,e^{-(7in+60)x/3R}\left[\frac{7(in - 60)}{3R}\left[G_0 + \frac{60ig_0}{n}(1 - e^{7inx/3R})\right] - \frac{140g_0}{R}e^{7inx/3R}\right] \qquad \ldots(50)$$

Now, by substituting these expressions obtained above for g' and G' into eqns. (37) and (39), we have

$$h_0 = \frac{1}{3}\, g_0^2 \, e^{-(280/R)x} - 12, \qquad \ldots(51)$$

and

$$h_1 = g_0 \, e^{-7(in+120)x/3R}\left[\left(\frac{in}{180} + \frac{2}{3}\right)\left[G_0 + \frac{60ig_0}{n}(1 - e^{7inx/3R})\right] - \frac{1}{3}\, g_0 \, e^{7inx/3R}\right] - (in + 12). \qquad \ldots(52)$$

By putting the expressions obtained above for u_0, u_1, v_0, v_1, h_0 and h_1 in (6), i.e., the perturbation assumed earlier for time dependent flow, the mathematical relations for velocity components u, v and pressure gradient parameter h can be obtained as:

$$u = 6(y - y^2)(1 + \epsilon \cos nt) + \left(y^3 - \frac{3}{2}y^2 + \frac{y}{2}\right)e^{-(140/R)x}\left[g_0 + \epsilon\left[\cos\left[n\left(t - \frac{7x}{3R}\right)\right]\left(G_0 + \frac{60\,g_0}{n}\sin\frac{7nx}{3R}\right) - \sin\left[n\left(t - \frac{7x}{3R}\right)\right]\frac{60\,g_0}{n}\left(1 - \cos\frac{7nx}{3R}\right)\right]\right] \quad ...(53)$$

$$v = \frac{35}{R}(y^4 - 2y^3 + y^2)e^{-(140/R)x}\left[g_0 + \epsilon\left[\cos\left[n\left(t - \frac{7x}{3R}\right)\right] \times \left[G_0 - g_0\left(1 - \frac{60}{n}\sin\frac{7nx}{3R}\right)\right] - \sin\left[n\left(t - \frac{7x}{3R}\right)\right] \times \left[\frac{60\,g_0}{n}\left(1 - \cos\frac{7nx}{3R}\right) + \frac{nG}{60}\right]\right]\right] \quad ...(54)$$

$$h = \frac{1}{3}g_0^2\,e^{-(280/R)x}\left[1 + \epsilon\left[\cos\left[n\left(t - \frac{7x}{3R}\right)\right]\left(2\frac{G_0}{g_0} - 1 + \frac{120}{n}\sin\frac{7nx}{3R}\right) - \sin\left[n\left(t - \frac{7x}{3R}\right)\right]\left[\frac{n\,G_0}{60\,g_0} + \frac{120}{n}\left(1 - \cos\frac{7nx}{3R}\right)\right]\right]\right] - 12(1 + \epsilon\cos nt) + n\,\epsilon\sin nt. \quad ...(55)$$

Finally using (53), the expressions for the non-dimensional shear stress parameters τ_0 and τ_1 at the inner and outer walls of bifurcation are obtained as under:

$$\tau_0 = \left(\frac{\partial u}{\partial y}\right)_{y=0} = A + 6(1 + \epsilon\cos nt) \quad ...(56)$$

$$\tau_1 = \left(\frac{\partial u}{\partial y}\right)_{y=1} = A - 6(1 + \epsilon\cos nt) \quad ...(57)$$

where

$$A = g_0 + \epsilon\left[\cos\left[n\left(t - \frac{7x}{3R}\right)\right]\left[G_0 + \frac{60g_0}{n}\sin\frac{7nx}{3R}\right] - \sin\left[n\left(t - \frac{7x}{3R}\right)\right]\frac{60\,g_0}{n}\left(1 - \cos\frac{7nx}{3R}\right)\right]$$

The results are reduced to the time-independent case for perturbation parameter (ϵ) to be of negligible small magnitude as were obtained by Zamir and Roach (1973). In addition, these expressions are consistent with the x-boundary condition (15) which requires that as $x \to +\infty$, the flow becomes fully developed Poiseuille flow.

5. Results and Discussion

The mathematical expressions obtained in above eqns. (53) to (57) for dimensionless velocity components, pressure gradient and shear stress parameters at

the inner and outer walls of bifurcation are dependent on the values of g_0 and G_0 (i.e., the flow conditions at the bifurcation apex). However, the results obtained here would be hypothetical in the present context, since in a real flow situation, the solid boundary and its bifurcating wall cannot have 'zero thickness' as is assumed to be the case for flat plate. Here, in real arterial bifurcation, the value of g_0 and G_0 will assume a high value depending upon the angle of bifurcation and the thickness of the bifurcating apex. So, if we assume the pressure gradient at the fork section the same as that in distant part of the trunk (i.e., $x=-\infty$), then by using the boundary conditions (14) and the relation (55) between h and g_0, and by comparing the constants and coefficients of ϵ, we find

$$g_0 = 3\sqrt{3}, \qquad \ldots(58)$$

and the relation

$$G_0 = \frac{(9+1/3g_0^2)\cos nt}{[2/3g_0 \cos nt - (ng_0/180)\sin nt]} \qquad \ldots(59)$$

respectively. Similarly, if we assume the pressure gradient at the fork section the same as that in the distant part of the branches (i.e., $x = +\infty$), and then using eqn. (15) and (55), we get

$$g_0 = 0 \text{ and } G_0 = 0. \qquad \ldots(60)$$

However, in view of the expected values of shear stress and pressure gradient parameters near the fork section, neither of these is a likely value of g_0 and G_0,

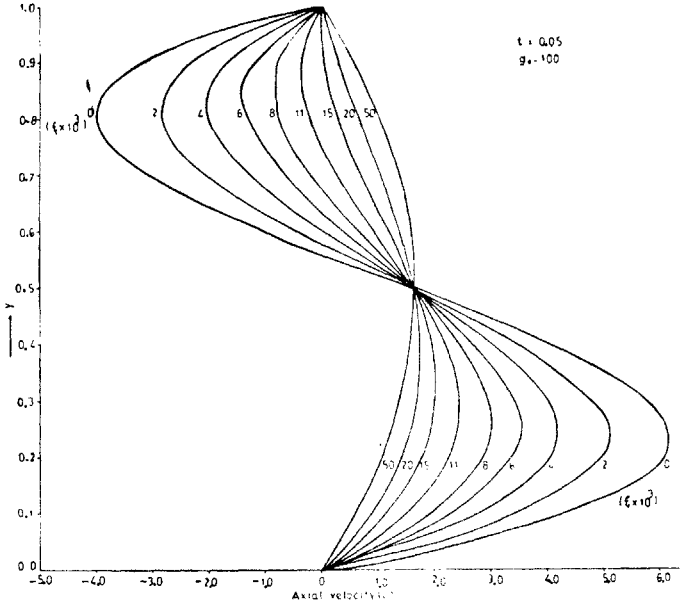

FIG. 2. Velocity profiles at different cross sections of a bifurcation branch for different values of ($\xi \times 10^3$), and for fixed values of dimensionless time (t) and g_0.

though it may concluded from these values that g_0 and the corresponding value of G_0 in general will be much higher since bifurcations in the real human system are much more complicated. Thus, we have computed the hemodynamic factors obtained in the previous section, with $\epsilon = 0.1$ for different values of g_0, dimensionless time (t) and the corresponding value of G_0 obtained from the relation (59). Moreover, in order to generalise this analysis for any Reynolds Number, we define a new parameter $\xi = x/R$ and present all the results in terms of ξ rather than x. For the same reason, the secondary velocity component (v) is also presented in terms of ($v \times R$)and ξ throughout this analysis rather than v and x.

The axial velocity profiles at different cross-sections of a bifurcation branch for $g_0 = 100$ and $t = 0.05$ are shown in Fig. 2. It may be noticed that for $(\xi \times 10^3) < 15$, a region of reverse flow develops near the outer wall, and that this region grows with

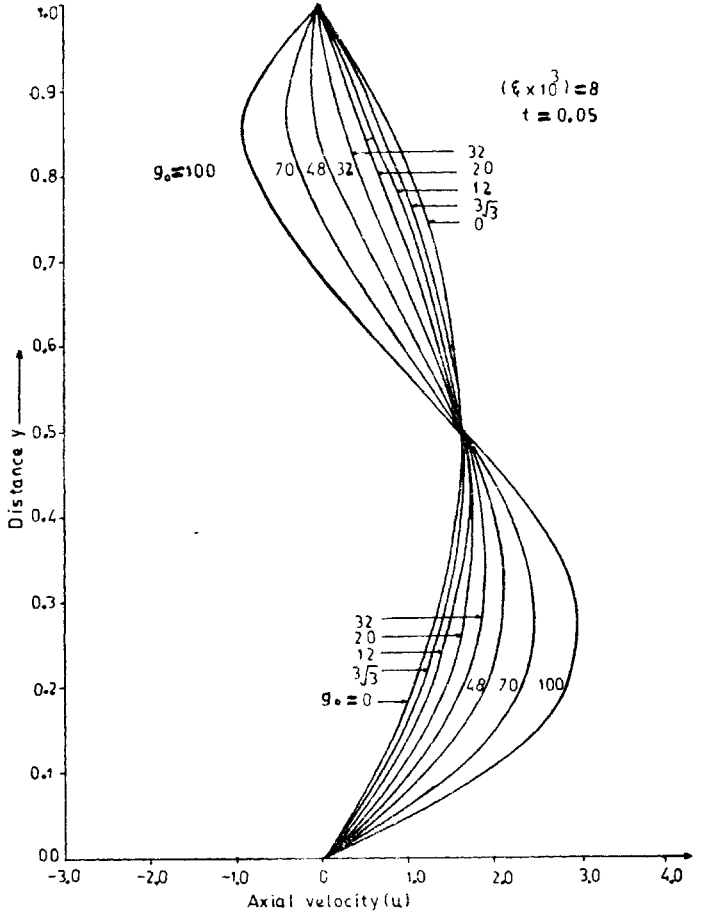

FIG. 3. Velocity profiles at the cross section ($\xi \times 10^3 = 8$) of a bifurcation branch for different values of g_0, and for fixed value of dimensionless time $t = 0.05$.

increase in the value of the parameter ($\xi \times 10^3$). These velocity profiles of u are also presented in Fig. 3 at the fixed cross-section (i.e., $\xi \times 10^3 = 8$) of a bifurcation branch for same value of dimensionless time (t) and for different values of g_0 i.e., for different types of bifurcations. It was observed that the region of reverse flow develops near the outer wall for $g_0 > 32$ and while Zamir and Roach (1973) observed this region of reverse flow for $g_0 > 12$ at the fork section (i.e., $\xi \times 10^3 = 0$) in their analysis for steady flow. The development in the x-direction of the secondary velocity profile (v) is shown in Fig. 4 for $g_0 = 100$ and fixed value of dimensionless time ($t = 0.05$). It is seen that each profile has a maximum at $y = 0.5$ and that the magnitude of this maximum is highest at the fork section.

The primary and secondary velocity profiles u and v at the fixed cross-section (i.e., $\xi \times 10^3 = 8$) of a bifurcation branch, with $g_0 = 100$ are shown in Figs. 5 and 6 for different values of dimensionless time (t). It was observed that the axial velocity component changes periodically with the change in the value of dimensionless time t. Further, it may also be noted from Fig. 5 that the region of back flow develops near the outer wall and this region varies periodically with respect to time. The periodic

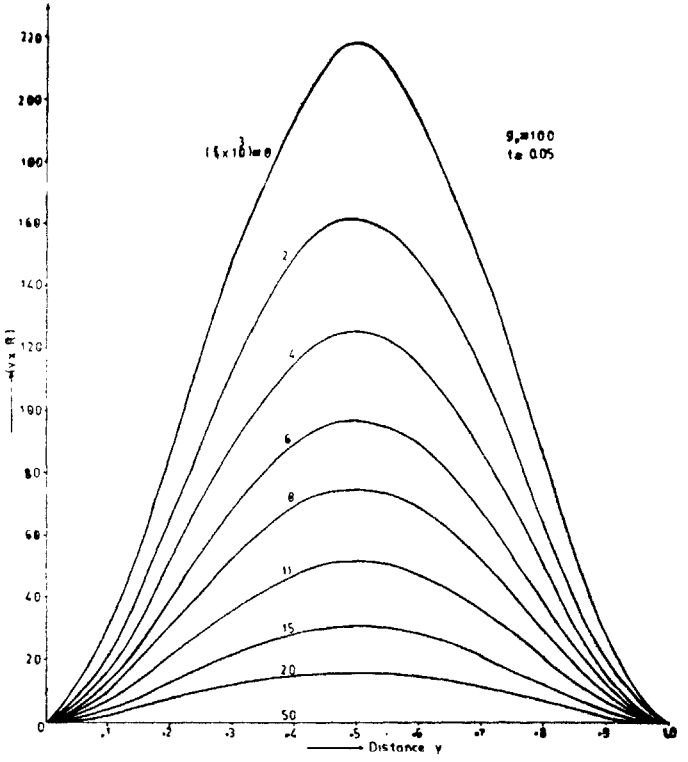

FIG. 4. Secondary flow (v) at different cross sections of a bifurcation branch (for different values of ($\xi \times 10^3$), and for fixed values of dimensionless time (t) and g_0.

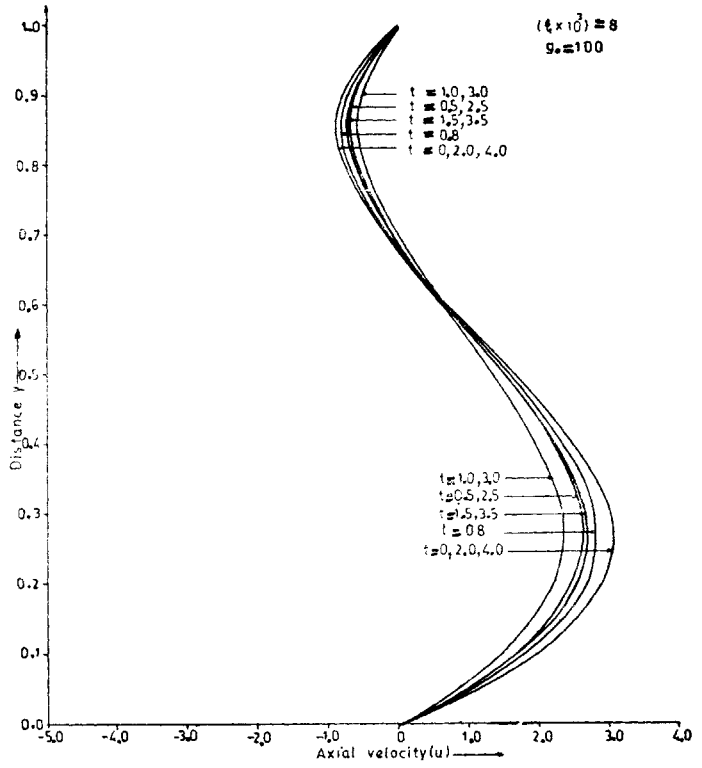

FIG. 5. Velocity profiles at the cross section ($\xi \times 10^3 = 8$) of a bifurcation branch for different values of dimensionless time (t) and for ($g_0 = 100$).

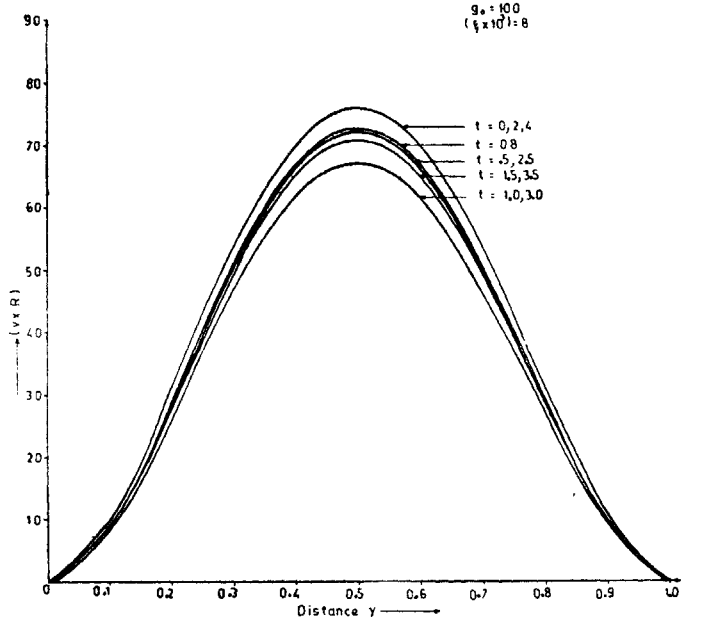

FIG 6. Secondary flow (v) at the cross section ($\xi \times 10^3 = 8$) of a bifurcation branch for different values of dimensionless time (t) and for $g_0 = 100$.

variation in the secondary velocity profile v was also observed with respect to time i. e., for $t = 0.0$, 2.0 and 4.0, we have one and the same profile. Moreover, it is also obvious from Fig. 6 that each profile has a maximum at $y = 0.5$ and that the magnitude of this maximum is highest after certain interval of time (i. e., the maximum is highest for $t = 0.0, 2.0, 4.0, \ldots$).

The development in the axial and secondary velocity profiles for different values of g_0 with respect to time is also shown in Figs. 7 and 8 at fixed cross-section (i.e., $\xi \times 10^3 = 8$) of a bifurcation branch. Figure 7 illustrates that the axial velocity component (u) decreases with decrease in the value of g_0 at fixed distances $y = 0.3$ and $y = 0.8$). Similar conclusion can be drawn from Fig. 8 for secondary velocity component (v) at fixed distance $y = 0.5$. Periodic variation in the velocity component u and v, is also observed with respect to time (t).

The distribution of shear stresses at the inner and outer walls of bifurcation is shown in Fig. 9 for different values of dimensionless time (t) and, for fixed value $g_0 = 100$. It is important to note that both τ_0 and τ_1 reach a maximum at the fork section (i.e., $\xi \times 10^3 = 0$) for all t. Moreover, Fig. 9 gives an idea of the distance, from the fork section at which the flow becomes a fully developed

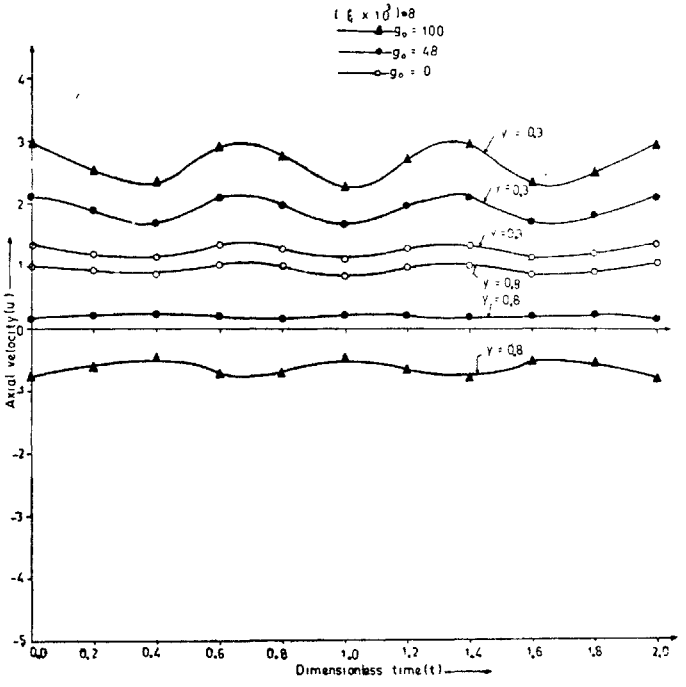

FIG. 7. Axial velocity component (u) with respect to time (t) at distances $y = 0.3$ and $y = 0.8$ for fixed cross section ($\xi \times 10^3 = 8$) of a bifurcation branch and for different values of g_0.

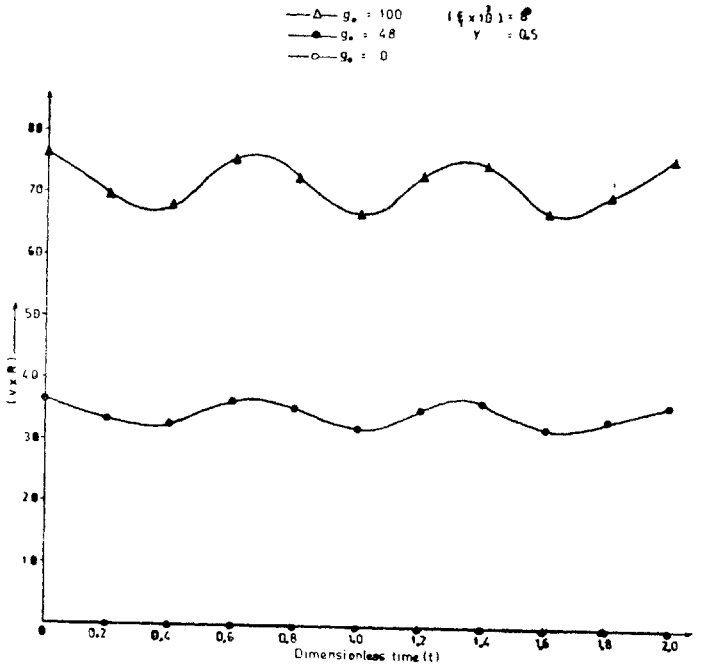

FIG. 8. Secondary flow (v) with respect to time (t) at distance $y = 0.5$ for fixed cross section ($\xi \times 10^3 = 8$) of a bifurcation branch and for different values of g_0.

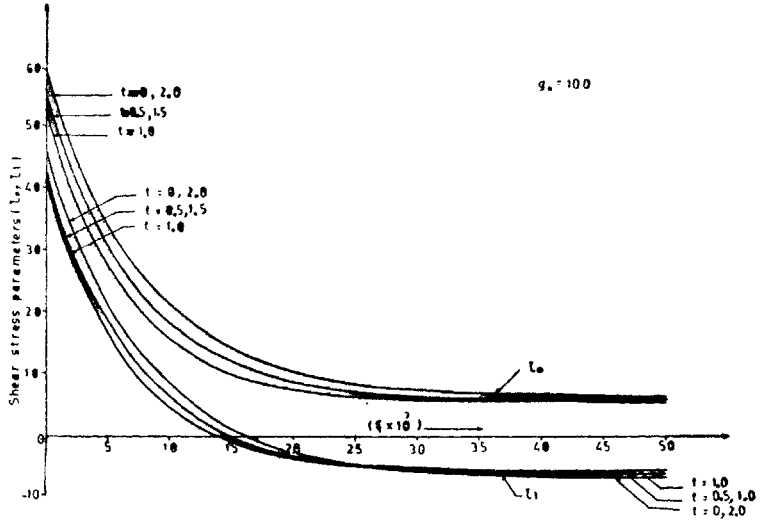

FIG. 9. Non-dimensional shear stress parameters τ_0 and τ_1 at different cross sections of a bifurcation branch for different values of dimensionless time (t) and for fixed value $g_0 = 100$.

Poiseuille flow in the branches for different values of dimensionless time (t). It may also be observed that the distribution of shear stress parameters is periodic with respect to time—for example the values of τ_0 and τ_1 are same for $t = 0$, 2 and 4. The variation of pressure gradient parameter (h) is presented in Fig. 10 for different values of g_0 and dimensionless time (t). As expected, it was observed that h becomes negative for $\xi \to \infty$ and becomes positive as $\xi \to 0$ and it reaches a maximum at the fork section. This figure also explains the effect of the values of g_0 and t on the magnitude of this maximum, and the distance downstream, from the fork section at which the flow becomes fully developed Poiseuille flow in branches. It depicts that pressure gradient varies periodically with respect to time and approaches its fully developed Poiseuille value asymptotically.

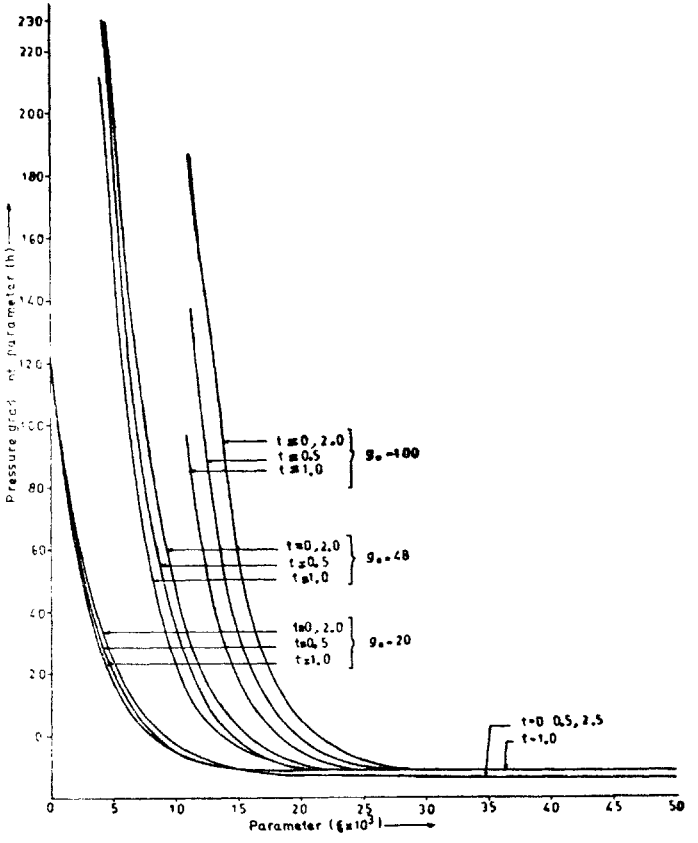

FIG. 10. Variation of pressure gradient parameter (h) in a bifurcation branch for different values of g_0 and dimensionless time (t).

The values of shear stress (τ_0 and τ_1) and the pressure gradient parameter (h) are plotted against dimensionless time (t) in Figs. 11 and 12 respectively, for fixed cross-section (i e., $\xi \times 10^3 = 8$) of a bifurcation branch and for fixed value of g_0. It was observed that the value of these parameters (τ_0, τ_1 and h) decrease with the decrease in the value of g_0. It also depicts that the periodic variation of shear stress parameters and pressure gradient parameter with respect to time increases with

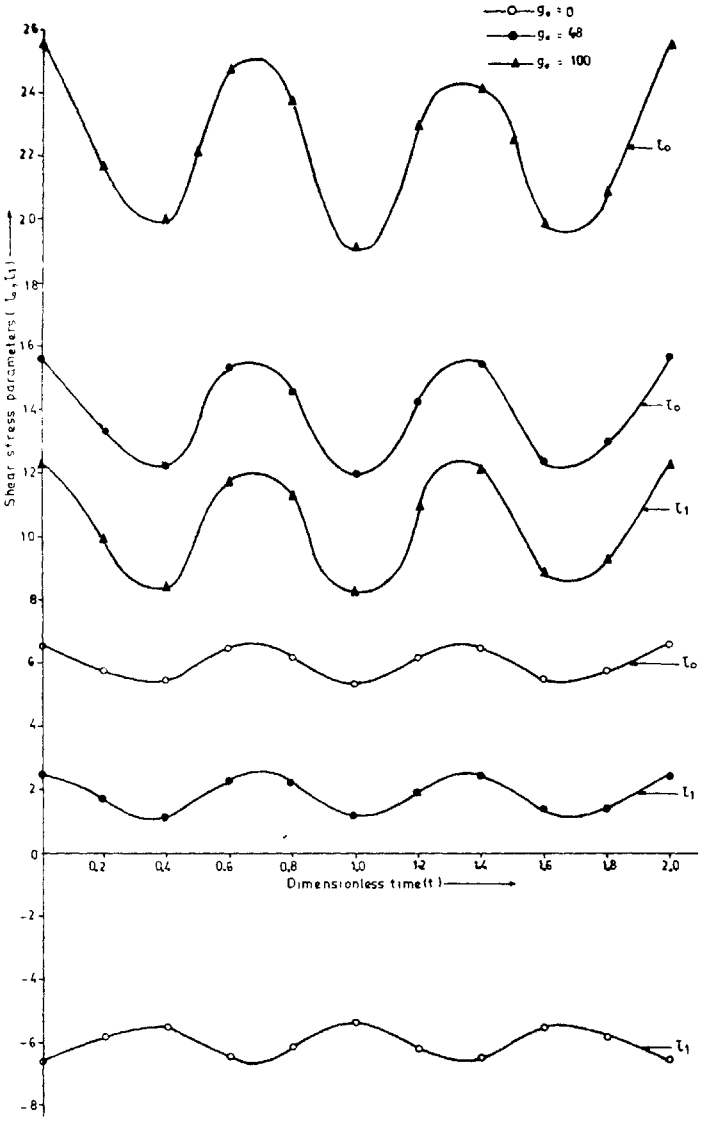

FIG. 11. Non-dimensional shear stress parameters (τ_0 and τ_1) vs. dimensionless time (t) at fixed cross section ($\xi \times 10^3 = 8$) of a bifurcation branch for different values of g_0.

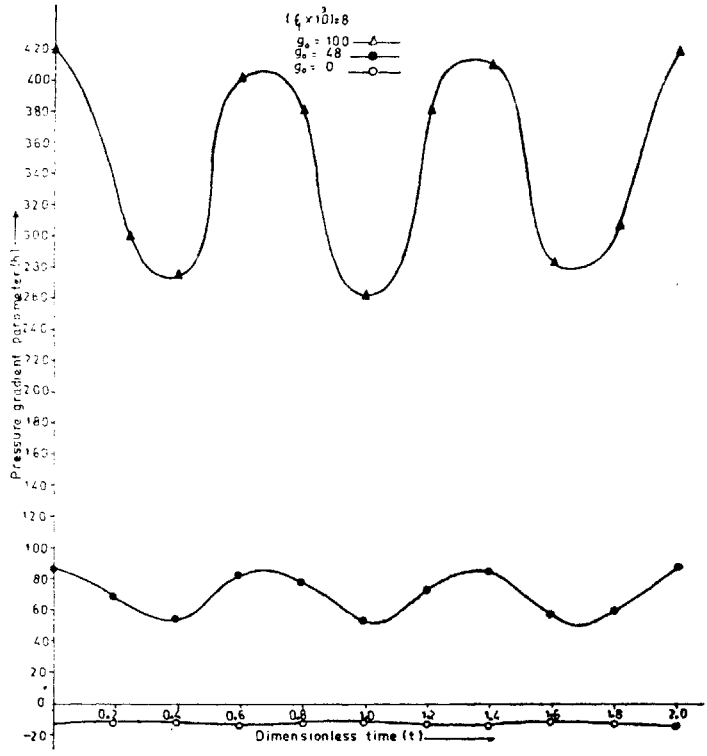

FIG. 12. Non-dimensional pressure gradient parameter (h) vs dimensionless time (t) at fixed cross section ($\xi \times 10^1 = 8$) of a bifurcation branch for different values of g_0.

increase in the value of g_0 (i.e., with the increase in shape and thickness of bifurcation).

Blockage effect at the apex of bifurcation is one of the important features from the pathological point of view of the flow in an arterial network system. It is caused by the development of boundary layers on the inner walls and a region of high shear near the apex of bifurcation. The magnitude of this 'blockage effect' is the value of pressure gradient at the fork section, from eqns. (3) and (55), is given by

$$\left(\frac{dp^*}{dx^*}\right)_{x^*=0} = \frac{\eta m}{2 b^3 \rho}\left[\left(\frac{1}{3} g_0^2 - 12\right) + \epsilon\left[\left(\frac{2}{3} g_0 G_0 - 12 - \frac{1}{3} g_0^2\right)\cos nt + n \sin nt \left(1 - \frac{g_0 G_0}{180}\right)\right]\right], \quad \ldots(61)$$

which reduces to the 'blockage effect' of steady case for perturbation parameter (ϵ) to be negligible magnitude as obtained by Zamir and Roach (1973). It is seen that

the effect will be much stronger when the branches are small in breadth/diameter and the rate of mass flow (m) is high. Also, since the value of g_0 in general be higher for smaller bifurcation angles, we may conclude that the blockage effect in general will be stronger at smaller bifurcation angles.

It is obvious that no definite medical conclusions can be drawn from this simulation because of the simplicity of the model. However, the hemodynamic parameters obtained above in equations (53) to (57) give an account of small fluctuations inevitable in any real solution. The fluctuating terms $(7x/3R)$ backs the fluctuations in the main stream which shows the ability of back flow near the walls of bifurcation. It can also deduced from these expressions that the fluctuations are maximum at the apex of bifurcation than as compared at distant part of the bifurcation. It is seen from figures for axial velocity profile u that with high fluctuations, the region of sluggish or back flow develops near the outer wall at the fork section. Thus, it can be predicted from the present analysis, that very different forces exist at the apex and at the lateral angles of bifurcation. It is also interesting to note from the figures that the flow is not only characterized by a velocity profile with a point of inflexion but is also constantly disturbed by the comparatively high secondary flow in that region. This observation is favourable for early transition to turbulent flow near the fork section (Schlichting 1968).

Hassler (1961) and Ferguson (1972) suggested on the basis of some in vitro experiments on isolated cerebral arteries, that hemodynamic forces like shear or pressure may probably cause the formation of aneurysms. Hassler (1962a 1962b) observed from their pathological studies that intimal cushions develop at the lateral angles of intracranial bifurcations due to the flow disturbances occurring in this area. The present model suggests that these may be due to decrease in shear or even to a zone of slow or back flow in this region. Fry (1968, 1969a, 1969b) proved with his experiments that high shear (approximately 400 dynes/cm) due to localized turbulence in dog aortas caused endothelial damage with increased penetration of both Evans blue dye and Chylomicra and remarked that high shear rates near bifurcations may be responsible for the development of atherosclerosis.

Therefore, it is evident from the above discussion that the present modelling may prove useful in separating the hemodynamic factors involved for time-dependent flow and interpreting the effect of only one factor at a time.

6. Conclusion

The present mathematical simulation will encourage medical researchers to deal with human blood circulation system more numerically along with their experiments. Another conclusion resulting from the analysis is that some hemodynamic forces, for example, shear forces etc., exist at the apex of bifurcation with the development of boundary layers on the inner walls of bifurcation. Such shear or pressure forces may lead to cardiovascular and neural lesions like, arteriosclerosis, intracranial aneurysms and intimal cushions etc. at and near the apex of bifurcation. Thus it will

be of great use in medical applications for diagnosing the above mentioned lesions by predicting and analysing the involvement of hemodynamic factors.

REFERENCES

Ferguson, G. G. (1972). Physical factors in the initiation growth and rupture of human intracranial saccular aneurysms. *J. Neurosurg.*, **37**, 666.

Forbus, W. D. (1930). On the origin of miliary aneurysms of superficial cerebral arteries. *Bull. John Hopkins Hosp.*, 47, 239.

Fry, D. L. (1968). Accute vascular endothelial changes associated with increased blood velocity gradients. *Circulation Res.*, **22**, 165.

——— (1969a). Certain chemo-rheologic considerations regarding the blood vascular interface with particular reference to coronary artery disease. *Circulation*, **40** (Suppl. 4), IV-38.

——— (1969 b). Certain histological chemical responses of the vascular interface to acutely induced mechanical stress in the aorta of the dog. *Circulation Res.*, **24**, 92.

Hassler, O. (1961). Morphological studies on the large cerebral arteries with reference to aetiology of subarachnoid haemorrhage. *Acta Neurol. Scand. Suppl.*, **154**, 1.

——— (1962a). Physiological intima cushions in the large cerebral arteries of young individuals (I-Morphological structure and possible significance for the circulation). *Acta Path. Microbiol. Scand.*, **55**, 19.

——— (1962b). Physiological intima cushions in the large cerebral arteries of young individuals (II-Location). *Acta Path. Microbiol. Scand*, **55**, 28.

——— (1963). Media defects in human arteries. Angiology, 14, 368.

Lighthill, M. J. (1954). The response of laminar skin friction and heat transfer to fluctuations in the stream velocity. *Proc. R. Soc.*, **A224**, 1.

Pool, J. L., and Potts, D. G. (1965). Aneurysms and Arteriovenous Anomalies of the Brain: Diagnosis and Treatment, Harper and Row, New York.

Roach, M. R., Scott, S., and Ferguson, G. G. (1972). The hemodynamic importance of the geometry of bifurcations in the circle of Willis. *Stroke*, **3**, 255.

Schlichting, H. (1968). Boundary Layer Theory. McGraw-Hili Book Co., Inc; New York. pp. 445.

Schroter, R. C., and Sudlow, M. F. (1969). Flow patterns in models of the human branched airways. *Resp. Physiol.*, 7, 341.

Stehbens, W.E. (1959). Turbulence of blood flow. *Quart. J. Expt. Physiol.*, 44, 110.

——— (1961). Discussion on vascular flow and turbulence, *Neourology* (*Minneapolis*), **11**, 66.

Zamir, M., and Roach, M. R. (1973). Blood flow downstream of a two dimensional bifurcation. *J. Theo. Biol.*, **42**, 33.